Optimal Control-Based Bayesian Detection of Clinical and Behavioral State Transitions

Sabato Santaniello, *Member, IEEE*, David L. Sherman, *Member, IEEE*, Nitish V. Thakor, *Fellow, IEEE*, Emad N. Eskandar, and Sridevi V. Sarma, *Member, IEEE*

***Abstract*—Accurately detecting hidden clinical or behavioral states from sequential measurements is an emerging topic in neuroscience and medicine, which may dramatically impact neural prosthetics, brain–computer interface and drug delivery. For example, early detection of an epileptic seizure from sequential electroencephalographic (EEG) measurements would allow timely administration of anticonvulsant drugs or neurostimulation, thus reducing physical impairment and risks of overtreatment. We develop a Bayesian paradigm for state transition detection that combines optimal control and Markov processes. We define a hidden Markov model of the state evolution and develop a detection policy that minimizes a loss function of both probability of false positives and accuracy (i.e., lag between estimated and actual transition time). Our strategy automatically adapts to each newly acquired measurement based on the state evolution model and the relative loss for false positives and accuracy, thus resulting in a time varying threshold policy. The paradigm was used in two applications: 1) detection of movement onset (behavioral state) from subthalamic single unit recordings in Parkinson's disease patients performing a motor task; 2) early detection of an approaching seizure (clinical state) from multichannel intracranial EEG recordings in rodents treated with pentylenetetrazol chemoconvulsant. Our paradigm performs significantly better than chance and improves over widely used detection algorithms.**

***Index Terms*—Bayesian estimation, neural systems, optimal control, quickest detection (QD).**

I. Introduction

THE detection of changes in a sequence of observations collected from a target system is of great interest in engineering [1]–[3], finance [4], [5], and the sciences [6]–[9]. Changes may be abrupt (i.e., fast with respect to the sampling period of the observations), small in amplitude, and stochastic (i.e., they impact the distribution of the observations), but account for remarkable changes in the system's state and properties [10], [11].

Manuscript received October 25, 2011; revised May 02, 2012; accepted July 05, 2012. Date of publication August 08, 2012; date of current version September 07, 2012. The work of S. V. Sarma was supported by the US National Science Foundation Career Award 1055560 and the Burroughs Wellcome Fund CASI Award 1007274. Date of publication August 08, 2012; date of current version September 07, 2012.

S. Santaniello, D. L. Sherman, N. V. Thakor, and S. V. Sarma are with the Department of Biomedical Engineering, Johns Hopkins University, Baltimore, MD 21218 USA (e-mail: ssantan5@jhu.edu; sherman@jhu.edu; nthakor@jhu.edu; ssarma2@jhu.edu).

E. N. Eskandar is with the Department of Neurosurgery, Massachusetts General Hospital, Boston, MA 02114 USA.

Color versions of one or more of the figures in this paper are available online at http://ieeexplore.ieee.org.

Digital Object Identifier 10.1109/TNSRE.2012.2210246

In the last 20 years, change point detection has gained interest in neuroscience and medicine (e.g., [12]–[39]), where precisely detecting physiological changes in clinical or behavioral expression is critical. For example, detecting an incoming epileptic seizure from early small electroencephalographic (EEG) changes before the appearance of clinical symptoms would result in timely warning to the patient or treatment with anticonvulsant drugs or neurostimulation. In brain–computer interface applications, one would like to accurately detect a change in the cortical activity due to motor planning before the movement (behavioral expression) is actually performed, so that such activity can drive an external prosthesis more naturally.

In these applications, the state transitions are hidden in neural measurements (e.g., EEG, single unit recordings, etc.) and impact statistics computed from these measurements. These state changes must be detected online (i.e., after every newly acquired measurement it must be decided whether or not the change has occurred) [11], and must minimize both the probability of a false positive (i.e., detection of an inexistent state transition) and the lag between actual and estimated change time for true positives [40], [41]. The most recent approaches to seizure detection and brain–machine interface have explored a wide range of tools in machine learning [18]–[25], artificial neural network [26]–[33], and estimation theory [34]–[39] to optimally detect a state change. However, no explicit performance specification or cost function has been introduced thus far and, because of this, the resultant detection algorithms often produce too many false positives when implemented online on test data [42].

We formulate the change point detection as a "quickest detection" (QD) problem [11], [40], [41] and solve it by developing a paradigm that combines hidden Markov models (HMM) [43], [44], Bayesian estimation [45], and optimal control [46]. First, we model the brain's activity as the output of a two-state HMM where the physiological output (e.g., EEG, spiking activity, etc.), which is due to the actual (not visible) clinical or behavioral state, is generated sequentially. Then, we recursively compute the *a posteriori* conditional probability of state transition given current and past observations (Bayesian estimation), where the condition on past observations takes into account the temporal dependencies that exist in neural data. Finally, we obtain the optimal detection policy (*ODP*) by minimizing a loss function of the expected distance between actual and detected change time (QD). The loss function weights separately early detection (i.e., before the actual change time, which may represent a false positive condition) and delayed detection (i.e., after the actual change time), thus penalizing differently the probability of false positives and true positives. This function depends

on both the probability of a state transition and the sequential measurements, and is minimized by solving an optimal control problem [46], [47].

We first validate our paradigm in simulations with observations generated by Bernoulli and Gaussian random processes. Then, we apply our paradigm on two experimental data sets: (i) spike trains from 34 neurons recorded in the subthalamic nucleus (STN) of seven Parkinson's disease (PD) patients before and during the execution of a movement [48]; (ii) multichannel intracranial EEG recordings (iEEG) simultaneously acquired in anterior and posterior thalamus, cortex, and hippocampus in a rodent model of generalized epilepsy (Sprague–Dawley rats treated with pentylenetetrazol [PTZ] chemoconvulsant) [49].

Since the STN neurons modulate their own spiking activity during the execution of voluntary motor tasks [48], [50]–[52], our paradigm ran on spike trains and detected the transition in spike distribution from rest to movement (behavioral state transition) in PD patients. In the acute rodent model of epilepsy, a time-varying power spectrum-based connectivity matrix among the iEEG channels was estimated and the correspondent sequence of first singular values was computed. Our paradigm ran on sequential measurements of the first singular value and provided an early detection (several minutes before the actual onset) of the incoming PTZ-evoked seizure (clinical state transition).

In both examples, we compared our approach to existing approaches to change point detection, including standard Bayesian Estimation [45], *CUSUM* [12], [13], [53], heuristic threshold, and a chance level predictor. In all cases our optimal detection scheme outperformed all approaches by 30%–400%.

Preliminary results were presented in [54] and [55]. Our approach was recently used in [56] to detect the seizure onset in drug resistant epileptic patients.

II. Materials and Methods

We develop the detection paradigm for a generic system $\mathcal{S}$, whose state is unknown. We assume that measurements (observations) of $\mathcal{S}$ are sequentially obtained at discrete stages $k = 0, 1, 2, \ldots$ The paradigm will then be applied to each dataset.

A. Hidden Markov Model and State Evolution

We assume that the observations z_k obtained from $\mathcal{S}$ at discrete stages $k = 0, 1, 2, \ldots$, may depend on previous observations, which are encompassed in the history sequence $H_k \triangleq \{z_0, z_1, \ldots, z_{k-1}\}$. At each stage $k \geq 0$, the observed system's activity is generated by the HMM in Fig. 1(a) and is in one of two states ($x_k = 0$ or $x_k = 1$).

A full characterization of the HMM includes (i) the probability of the initial state $p_0 \triangleq P(x_0 = 1)$, (ii) the conditional probability of state transition, $p_k \triangleq P(x_k = 1 | x_{k-1} = 0)$, for all k, and (iii) the probability of the output measurement $q_x(z|H_k) \triangleq P(z_k = z | x_k = x, H_k)$, for any $x \in \{0, 1\}$, history H_k, and value z of interest [43]. Depending on the specific application, these probabilities can be estimated offline on training data. With this formulation, we assume that the state x_k is not visible and "hidden" in the observations z_k, which are available at every stage and depend probabilistically on x_k and H_k.

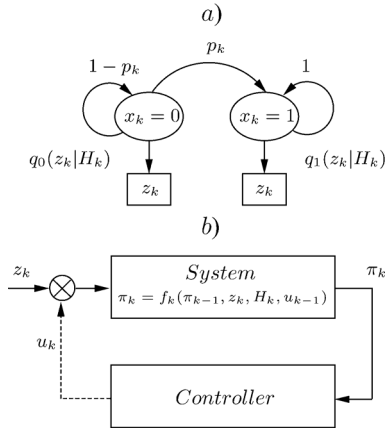

Fig. 1. (*a*) HMM schematic with two hidden states ($x_k = 0$ and $x_k = 1$) and observable output z_k, $k = 1, 2, \ldots$ p_k and $q_x(z_k|H_k)$ are the probability of transition from state 0 to state 1 and the probability function of z_k in state $x \in \{0, 1\}$ conditioned on the past output sequence H_k, respectively. (*b*) Change point detection formulated as a feedback control problem. π_k and u_k are the information state variable and the decision variable, respectively.

The goal of our paradigm is to detect the transition time $\overline{T} > 0$ from state 0 to state 1. Note that, because of the HMM, $\overline{T}$ is a discrete random variable, whose probability mass function is $P(\overline{T} = k) = p_k \prod_{j=0}^{k-1}(1 - p_j)$. We first introduce the Bayesian *information state variable* $\pi_k \triangleq P(x_k = 1 | z_k, H_k)$, which is the *a posteriori* probability of being in state 1 at stage k given the measurements up to and including stage k. It is straightforward to show that π_k evolves at each stage k recursively, based on the current and past observations (z_k and H_k, respectively), the probability p_k of a state transition in the HMM and the ratio $L_k \triangleq q_1(z_k|H_k)/q_0(z_k|H_k)$

$$\begin{aligned}\pi_0 &= P(x_0 = 1|z_0) = \frac{q_1(z_0)p_0}{q_1(z_0)p_0 + q_0(z_0)(1-p_0)} \\ \pi_{k+1} &= \frac{L_{k+1}\left[\pi_k + \xi_k p_{k+1}\right]}{(1-p_{k+1})\xi_k + L_{k+1}\left[\pi_k + \xi_k p_{k+1}\right]} \\ &\triangleq \Phi_{k+1}(\pi_k, z_{k+1}, H_{k+1}) \end{aligned} \tag{1}$$

where $\xi_k \triangleq 1 - \pi_k$. Equation (1) has been derived in [10], [17], [40], [41] in different ways. A possible derivation is reported in Appendix A.

B. Optimal Detection Policy (ODP)

Given a (finite) time horizon $M > 0$, the transition detection problem is an online decision problem that at each stage $k < M$ must test the hypothesis $\mathcal{H} \triangleq \{\overline{T}\ has\ occurred\}$, conditioned on the observations (H_k, z_k). We want to solve this problem by explicitly minimizing the loss function

$$\begin{aligned} J_0 \triangleq\ & a_1 E_{\overline{T}}\{\varphi(\overline{T} - T_S)\} P(\overline{T} > T_S) \\ & + a_2 E_{\overline{T}}\{\varphi^2(T_S - \overline{T})\} P(\overline{T} \leq T_S) \end{aligned} \tag{2}$$

where $\varphi(\epsilon)$ is a user-defined, nonnegative, nondecreasing function of the distance ϵ between the estimated (T_S) and actual ($\overline{T}$) change time, with $\epsilon \triangleq \overline{T} - T_S$ or $\epsilon \triangleq T_S - \overline{T}$ in the case of early ($\overline{T} > T_S$) or delayed ($\overline{T} \leq T_S$) detection, respectively, and $\varphi(\epsilon) = 0$ for $\epsilon < 0$. $E_{\overline{T}}\{\cdot\}$ is the expected value and parameters $a_1, a_2 > 0$ allow to tradeoff between early versus delayed

detection. Note that, depending on the application, $\overline{T} > T_S$ can either indicate a false positive (if $\overline{T}$ does not occur) or an early detection (if $\overline{T}$ does occur). Also, we note that the absolute distance $|\overline{T} - T_S|$ is weighted differently in case of early versus delayed detection (linear versus quadratic value of φ). This choice is made in order to penalize long delays (i.e., $T_S \gg \overline{T}$), as these events are usually unacceptable in most of the applications of interest in neuroscience and medicine.

Because the evolution of π_k does not matter anymore after that $\mathcal{H}$ has been accepted, we introduce the decision variable $u_k \in \{0, 1\}$, where $u_k = 0$ ($u_k = 1$) means that the hypothesis $\mathcal{H}$ is rejected (accepted) at stage k. In this way, we have

$$\begin{aligned}\pi_{k+1} &= f_{k+1}(\pi_k, z_{k+1}, H_{k+1}, u_k) \\ &\triangleq \begin{cases} \Phi_{k+1}(\pi_k, z_{k+1}, H_{k+1}), & u_k = 0 \\ termination, & u_k = 1 \end{cases}\end{aligned} \tag{3}$$

where the "*termination*" state simply implies that we have stopped caring about the observations z_k. Then, the detection results in deciding when to switch from $u_k = 0$ to $u_k = 1$ [46], [47] in order to minimize (2) and the solution is achieved via feedback control of our HMM system, where u_k is the control variable [Fig. 1(b)].

To construct the loss function (2) in terms of systems variables, we first define a loss-per-stage $G_k(\pi_k, u_k)$ that penalizes both rejecting $\mathcal{H}$ after that the state transition has occurred ($k > \overline{T}$), and accepting $\mathcal{H}$ before that the state transition occurs ($k < \overline{T}$), and it is 0 otherwise. This loss-per-stage is conditioned on the observations (H_k, z_k) and defined as follows:

$$G_k(\pi_k, u_k) \triangleq \begin{cases} a_2 E_{\overline{T}}\{\varphi(k - \overline{T})\}\pi_k, & u_k = 0 \\ a_1 E_{\overline{T}}\{\varphi(\overline{T} - k)\}\xi_k, & u_k = 1 \\ 0, & \text{otherwise} \end{cases} \tag{4}$$

where $\xi_k \triangleq 1 - \pi_k$ and we set $G_k(\pi_k, u_k) = 0$ if the switch from $u_k = 0$ to $u_k = 1$ has occurred before the stage k. We also introduce a terminal loss for rejecting $\mathcal{H}$ over the whole observation horizon $[0, M)$

$$G_M(\pi_M) = \begin{cases} a_1 E_{\overline{T}}\{\varphi(\overline{T} - M)\}\xi_M, & u_{M-1} = 0 \\ 0, & \text{otherwise} \end{cases}$$

where $\xi_M \triangleq 1 - \pi_M$. It is straightforward to show that, for any policy $(u_0 = \cdots = u_{T_S - 1} = 0, u_{T_S} = 1)$, minimizing the loss function (2) corresponds to minimizing the loss function

$$E_{z_0, z_1, \ldots, z_M}\left\{ G_M(\pi_M) + \sum_{k=0}^{M-1} G_k(\pi_k, u_k) \right\} \tag{5}$$

provided that φ is nondecreasing. We note that, in this formulation, M is finite as we restrict the detection problem to the class of decision policies that stop almost surely (i.e., with probability 1) in finite time. This choice guarantees that the cumulative loss (5) is finite and is consistent with most clinical applications of interest. Also, we note that $G_k(\pi_k, 0)$ is proportional to the derivative of the loss for delay in (2). In this way, the cumulative loss (5) gives a discrete time representation of the quadratic term in (2).

Minimization of the loss (5) can be achieved recursively by using dynamic programming [46]

$$J_M(\pi_M) = G_M(\pi_M) \tag{6}$$

$$\begin{aligned} J_k(\pi_k) = \min\Big\{ & G_k(\pi_k, u_k = 1),\ G_k(\pi_k, u_k = 0) \\ & + E_{z_{k+1}}\big\{ J_{k+1}\big(\Phi_{k+1}(\pi_k, z_{k+1}, H_{k+1})\big) | H_{k+1} \big\} \Big\} \end{aligned} \tag{7}$$

with $H_{k+1} \triangleq (H_k, z_k)$. By using (4), we have

$$\begin{aligned} J_k(\pi_k) = \min\Big\{ & a_1 E_{\overline{T}}\{\varphi(\overline{T} - k)\}\xi_k, a_2 E_{\overline{T}}\{\varphi(k - \overline{T})\}\pi_k \\ & + E_{z_{k+1}}\big\{ J_{k+1}\big(\Phi_{k+1}(\pi_k, z_{k+1}, H_{k+1})\big) | H_{k+1} \big\} \Big\} \end{aligned}$$

and the optimal solution is finally

$$T_{ODP} = \min\Big\{ 0 < k < M | \pi_k > F_k(\pi_k, z_k, H_k) \Big\} \tag{8}$$

where

$$\begin{aligned} F_k(\pi_k, z_k, H_k) &\triangleq \frac{a_1 E_{\overline{T}}\{\varphi(\overline{T} - k)\} - \Omega_{k+1}}{a_1 E_{\overline{T}}\{\varphi(\overline{T} - k)\} + a_2 E_{\overline{T}}\{\varphi(k - \overline{T})\}} \\ \Omega_{k+1} &\triangleq E_{z_{k+1}}\big\{ J_{k+1}\big(\Phi_{k+1}(\pi_k, z_{k+1}, H_{k+1})\big) | H_{k+1} \big\} \\ &= \sum_z J_{k+1}\big(\Phi_{k+1}(\pi_k, z, H_{k+1})\big) \\ &\quad \times P(z_{k+1} = z | H_{k+1}) \\ &= \sum_z J_{k+1}\big(\Phi_{k+1}(\pi_k, z, H_{k+1})\big) \Psi_{k+1} \\ \Psi_{k+1} &\triangleq q_1(z | H_{k+1})\big(\pi_k + \xi_k p_{k+1}\big) \\ &\quad + q_0(z | H_{k+1})\big(1 - p_{k+1}\big)\xi_k \end{aligned}$$

and the summation is taken over all the possible values z of z_{k+1}.

For sake of simplicity, we chose the linear penalty $\varphi(\epsilon) = 2\epsilon - 1$ for every application in this study, even though the paradigm is independent of the specific choice of $\varphi(\cdot)$. Also, we note that the threshold $F_k(\pi_k, z_k, H_k)$ evolves as a function of the current stage k, state π_k and the current and past measurements (z_k, H_k). $F_k(\cdot)$ is computed on line at each stage and, because the term Ω_{k+1} may be nonlinear, is not monotonic, i.e., it either increases or decreases based on the evolution of π_k and z_k.

C. Significance and Performance Tests

For each data set, the *ODP* (8) was compared to the following predictors.

- *Chance Level (CL) Predictor*. Only *a priori* information about the random variable $\overline{T}$ (change point) is exploited. The estimation T_{CL} is the mean of $\overline{T}$, i.e., $T_{CL} \triangleq E\{\overline{T}\}$.
- *Bayesian Estimator (BE)*. Only the probability π_k is used for deciding, at each stage k, whether the state transition has occurred or not. The estimation T_{BE} is given as soon as $\pi_k > 1 - \pi_k$, i.e., $T_{BE} \triangleq \min\{0 < k < M | \pi_k > 0.5\}$ [10], [45].

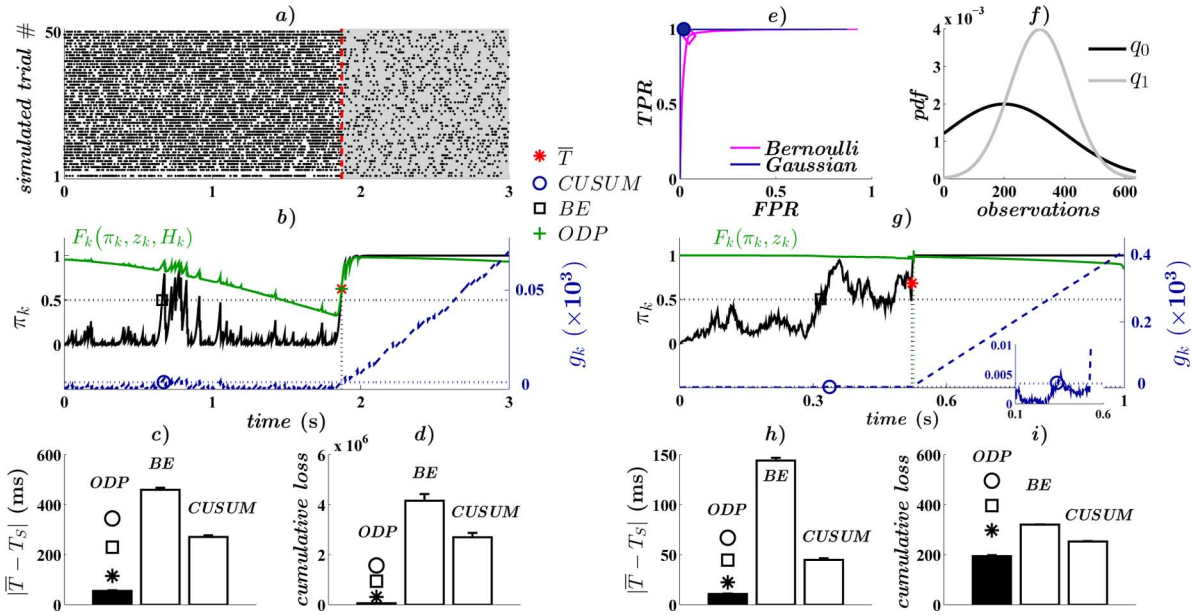

Fig. 2. Numerical simulations with Bernoulli (*a*)–(*e*) and Gaussian (*e*)–(*i*) processes. a) Raster of a Bernoulli process (one row per trial) in state 0 and 1 (white and gray background, respectively) aligned to the change time $\overline{T}$ (red line). (*b*) State variable π_k (black), *ODP* threshold $F_k(\cdot)$ (green), *CUSUM* variable g_k (blue dashed), and threshold $\overline{g}$ (blue dotted) computed for a single trial in (*a*). Time scale in (*b*) also applies to (*a*). (*c*), (*h*) Average distance between the estimated (T_S) and actual ($\overline{T}$) change time for each policy ($\text{mean} \pm \text{s.e.m.}$) in case of Bernoulli and Gaussian processes, respectively. (*d*), (*i*) Average loss $J \triangleq G_{T_S}(\pi_{T_S}, 1) + \sum_{i=0}^{T_S-1} G_i(\pi_i, 0)$ ($\text{mean} \pm \text{s.e.m.}$) for each policy in case of Bernoulli and Gaussian processes, respectively. In (*c*), (*d*), (*h*), (*i*), T_S varies with the policy. Asterisk, square, and circle denote significant differences ($p < 0.05$) *ODP* versus *CL*, *BE*, and *CUSUM*, respectively. (*e*) Average ROC curve for the *CUSUM* predictor estimated on Bernoulli and Gaussian processes, respectively. Diamond and circle denotes the point of the curve correspondent to the threshold $\overline{g}$ in (*b*) and (*g*), respectively. (*f*) Probability distribution function (*pdf*) of the Gaussian processes in state 0 (q_0) and 1 (q_1) (*g*) Plot as in (*b*) for a single trial of the Gaussian process. *Inset*: zoom around the *CUSUM* estimation. Legend in (*b*), (*g*) reports $\overline{T}$ and the estimation given by *ODP*, *BE*, and *CUSUM*.

- *Cumulative Sum Estimator (CUSUM)*. The log-likelihood ratio $l_k \triangleq log\Big(q_1(z_k|H_k)/q_0(z_k|H_k)\Big)$ is computed at each stage k and used to recursively update the information state variable g_k [10], [12], [13], [53]

$$g_0 \triangleq 0$$
$$g_k \triangleq \begin{cases} g_{k-1} + l_k, & \text{if } g_{k-1} + l_k > 0 \\ 0, & \text{otherwise.} \end{cases}$$

  A change point is detected if $g_k > \overline{g}$, with $\overline{g}$ chosen heuristically, i.e., $T_{CUSUM} \triangleq \min\{0 < k < M | g_k > \overline{g}\}$.
- *Heuristic Threshold-based Detector (HT)*. In the epilepsy example, we also implemented the policy $T_{HT} \triangleq \min\{0 < k < M | z_k > \overline{h}\}$, which detects a change point as soon as the output measurement z_k is above a fixed threshold $\overline{h}$.

For each data set, we chose $\overline{g}$ offline. First, for each sequence of observations in the data set, we tested several candidate thresholds $g > 0$ and, for each g, we counted how many stages k satisfied the condition $\{x_k = 1,\ g_k > g\}$ or $\{x_k = 0,\ g_k > g\}$ in that sequence. Then, we defined the false positive rate (*FPR*) and true positive rate (*TPR*) as functions of g

$$FPR(g) \triangleq \frac{\#\text{ of stages such that } \{x_k = 0,\ g_k > g\}}{\#\text{ of stages such that } \{x_k = 0\}}$$
$$TPR(g) \triangleq \frac{\#\text{ of stages such that } \{x_k = 1,\ g_k > g\}}{\#\text{ of stages such that } \{x_k = 1\}}.$$

Secondly, for each value of g, we computed the average false positive rate $\overline{FPR}(g)$ and average true positive rate $\overline{TPR}(g)$ across the available sequences of observations and then constructed the average receiver-operating characteristic (ROC) curve [57], i.e., we plotted $\overline{TPR}$ versus $\overline{FPR}$ for the various values of g. Finally, we chose $\overline{g}$ to maximize $\overline{TPR} - \overline{FPR}$ on the average ROC curve, i.e.,

$$\overline{g} \triangleq \min\left\{ \arg\max_{g>0} \left[\overline{TPR}(g) - \overline{FPR}(g) \right] \right\}.$$

The threshold $\overline{h}$ for the *HT* detector was chosen with a similar procedure. This choice of $\overline{g}$ and $\overline{h}$ aimed at achieving high *TPR* and low *FPR* values across multiple sequences of observations for the *CUSUM* and *HT* policy, respectively. High *TPR* values indicate that the detection policy is highly sensitive to the change points, while low *FPR* values imply that false positives and early detections are very unlikely events.

D. Numerical Simulations

Our paradigm was tested in simulation both on binary and continuous stochastic processes (Bernoulli and Gaussian random processes, respectively).

1) Bernoulli Processes: We simulated the HMM [Fig. 1(a)] $n = 5000$ times with $p_k = \rho = 0.001$ and $0 < k \leq M = 3000$. Note that, because p_k is constant, the change time $\overline{T}$ is a geometric random variable with $P(\overline{T} = k) = \rho(1-\rho)^{k-1}$. The initial condition was $p_0 = 0$, i.e., the HMM was initially in state $x = 0$. In each state, the observations z_k were Bernoulli processes with a refractory period, i.e., z_k was either 0 or 1

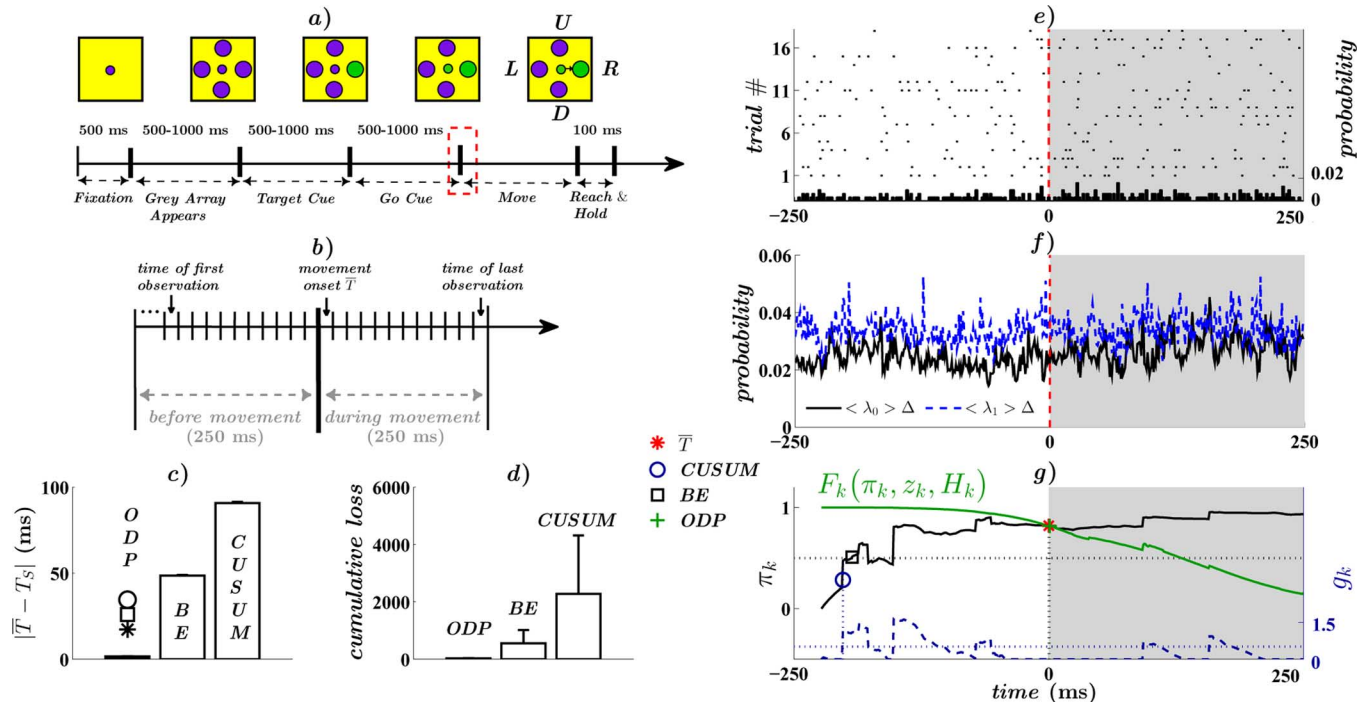

Fig. 3. Movement onset detection in PD patients. (*a*) Schematic of the reach-out task. Patients were requested to move the cursor toward the position indicated on the monitor (green large circle; four options: $U = \text{up}$; $D = \text{down}$; $L = \text{left}$; $R = \text{right}$) when the "Go Cue" signal (green small circle) appeared. For each successful task, we used STN single unit recordings (spike train) during 500 ms around the movement onset $\overline{T}$ (red box). (*b*) The movement onset times are forced to follow a geometric distribution. (*c*), (*d*) Population-averaged distance and loss as in Fig. 2, respectively. Asterisk, square, and circle denote significant difference ($p < 0.05$) *ODP* versus *CL*, *BE*, and *CUSUM*, respectively. (*e*) Top: example of STN neuron raster (patient PD-7) during several tasks aligned such that 0 denotes the movement onset (red). Each line refers to a single trial. Bottom: peri-event time histogram of the neuron associated with the raster. (*f*) Average instantaneous spike probability $\langle \lambda_x(k|H_k) \rangle \Delta$ in state $x = 0$ and $x = 1$ with $\Delta = 1$ ms and $\langle \cdot \rangle$ denoting, for each k, the average across the trials in (*e*). (*g*) Variable π_k (black), *ODP* threshold $F_k(\cdot)$ (green), *CUSUM* variable g_k (blue dashed), and threshold $\overline{g}$ (blue dotted) for a single trial from (*e*). Legend reports the actual change time $\overline{T}$ and the estimation given by *ODP*, *BE*, and *CUSUM*. Time scale in (*g*) also applies to (*e*) and (*f*).

and the distance between two consecutive 1 s was at least one stage, which means that the history H_k reduced to the previous observation z_{k-1} at each stage. The probability of observing 1 at the generic stage k in state $x \in \{0, 1\}$ was $q_x(z_k = 1|H_k) = \widehat{\lambda}_x(1 - z_{k-1})\Delta$, with parameter $\widehat{\lambda}_x$ being the average rate and Δ the duration of each stage. We set $\widehat{\lambda}_0 = 0.1$, $\widehat{\lambda}_1 = 0.02$, and $\Delta = 1$ ms [see Fig. 2(a)].

2) Gaussian Processes: We simulated the HMM [Fig. 1(a)] $n = 5000$ times with $p_k = \rho = 0.002$, $0 < k \leq M = 1000$, and $p_0 = 0$. The observations z_k were Gaussian processes with no dependency from the previous history, i.e., $z_k \sim \mathcal{N}(\widehat{\mu}_x, \widehat{\sigma}_x)$ with mean $\widehat{\mu}_x$ and standard deviation $\widehat{\sigma}_x$ depending on the state $x \in \{0, 1\}$. We set $\widehat{\mu}_0 = 200$, $\widehat{\sigma}_0 = 200$, $\widehat{\mu}_1 = 318$, and $\widehat{\sigma}_1 = 100$ [see Fig. 2(f)].

E. Movement Onset Detection From Spike Trains in STN Neurons

1) Experimental Setup: Seven patients undergoing deep brain stimulator placement for the treatment of Parkinson's disease (PD) were included in this study. The experimental setup was presented in [48]. Briefly, patients were awake in the operating room and performed a directed hand movement task [reach-out task, Fig. 3(a)] while single unit recordings were acquired from the subthalamic nucleus (STN). Patients viewed a computer monitor and moved a joystick with the hand contralateral to the recorded site once cued by a visual target. Each patient repeated the task several times while multiple STN neurons were simultaneously recorded. For each trial, the position of the target on the monitor and the delay (ranging from 500 to 1000 ms) between the task onset, the display of the target (target onset), and the display of the visual cue, were randomly chosen. The onset of each movement was determined by examining the joystick voltage acquired during the task. The STN neuronal activity was recorded through tungsten microelectrodes, band-pass filtered (0.3–6 kHz) and sampled at 20 kHz. Spikes were sorted offline using a standardized template-matching algorithm (Cambridge Electronics Design, Cambridge, U.K.). The number of STN neurons recorded and the number of trials repeated for each patient are reported in Table I.

TABLE I
TRIALS AND NEURONS PER PD PATIENT

Patient	# of Trials	# of Neurons
PD-1	235	5
PD-2	94	4
PD-3	141	6
PD-4	36	4
PD-5	122	5
PD-6	189	7
PD-7	38	3
TOTAL	855	34

2) HMM Fitting: For each trial and neuron, we considered a 500 ms peri-movement interval [250 ms before, 250 ms after

the movement onset, Fig. 3(a)] and denoted with state 0 and 1 the activity before and after the movement onset, respectively. We sampled the time horizon in consecutive 1-ms-long bins and set the observation z_k to be either 1 or 0 depending on whether the neuron spiked or not in the kth bin. Sarma *et al.* [48] showed that, in both states, every neuron in this data-set can be modelled as a point process [58] and that the conditional probability of a spike in a given time bin k depends on the spiking activity H_k in the last 150 bins before k. An approximated expression of this conditional probability is $q_x(z_k = 1|H_k) \cong \lambda_x(k|H_k)\Delta$, where $\Delta = 1$ ms is the size of the bin and $\lambda_x(k|H_k), x \in \{0, 1\}$, is the instantaneous spiking rate (conditional intensity function) in each state [58], [59]. For each neuron and state, a generalized linear model [60] captured the relationship between $\lambda_x(k|H_k)$ and the spiking history H_k (see Appendix B and [48] for model description and motivations).

For each spike train, we started the observations in state $x = 0$ and forced the movement onset (i.e., the transition time $\overline{T}$) to follow a geometric distribution by running a geometric process with $\rho = 0.0125$, picking a number $0 \leq t_0 < 250$ from this process, and then choosing the initial observation $250 - t_0$ ms before the movement onset [Fig. 3(b)].

F. Multichannel iEEG Recordings from PTZ-treated Rodents

1) Experimental Setup: Two male Sprague-Dawley rats (250–300 g) were treated with PTZ chemoconvulsant to elicit epileptic seizures. The experimental setup was presented in [49]. Briefly, each rodent was implanted with four skull screw EEG electrodes bifrontally and posteriorly behind bregma. Electrodes were bipolar insulated steel (0.125 mm diameter, 2 mm tip separation) placed on cortex (CTX), in anterior thalamus (AN) (two electrodes, one per side), and posterior thalamus (PT). A fifth depth electrode was in hippocampus (HPC). Animals recovered for two days with ad lib food and water. Then, they were implanted with a jugular venous catheter and recovered for a minimum of 1 h. Baseline iEEG signals were recorded for at least 60 s prior to the infusion of PTZ (100 $\mathrm{mg\ ml^{-1}}$, Sigma Chemical, St. Louis, MO), administered at 5.5 $\mathrm{mg\ kg^{-1}\ min^{-1}}$.

Behavior and iEEG signals were both continuously monitored in each rodent and the extent of the seizures was evaluated according to the modified clinical Racine scale [49], i.e., 0: no seizure, 1: oral facial twitch, 2: head bob, 3: myoclonic jerk, 4: forelimb clonus, 5: rearing clonic, and 6: rearing and falling clonic with forelimb clonus. Each animal passed through all the stages of the Racine scale.

Analogical iEEG recordings were simultaneously acquired from the five electrodes during seven nonconsecutive sessions (min and max session duration: 12 and 58 min, respectively; average: 33.0 ± 5.3 min, $\mathrm{mean} \pm \mathrm{standard\ error\ of\ mean}$ [s.e.m.]), and 12 seizures were hand-annotated. For each seizure, onset and offset were determined from the iEEG recordings visually by identifying high-amplitude, high-frequency oscillations, progressing into clonic paroxysmal discharges of lower frequency toward the end.

Signals were amplified with a Grass 8D-10 eight-channel portable polygraph with internal $[0.3,\ 70]$ Hz band-pass filter. A 60 Hz notch filter was also employed. Signals were collected with a seven-channel FM data recorder (TEAC MR-30) and digitized using CODAS software (DATAQ Instruments Inc., Akron, OH) with 1 kHz sampling rate. Signals were then digitally downsampled at 200 Hz offline.

2) Relevant Statistic and HMM Fitting: A time-varying connectivity matrix, A_k, characterized the pair-wise correlations among the five digitized iEEG series at each observation stage k. For each session, we chopped the iEEG series from each channel into consecutive 3-s-long windows (i.e., 600 samples per window) with 0.5 s overlap. Then, we defined A_k as a 5×5 matrix whose generic (i, j)th element is the cross-power in the band [80,100] Hz of the ith and jth channel in the kth window.

For each A_k, we computed the first (maximum) singular value $\sigma_1(k)$ [61] and assumed that this series is the output of the HMM, i.e., we set $z_k \triangleq \sigma_1(k)$, $k = 1, 2, \ldots$, with $x = 0$ and $x = 1$ being the baseline seizure-free (nonictal) and the seizure (ictal) condition, respectively. Motivations for the use of $\{\sigma_1(k)\}$ are in [54], [56], where $\{\sigma_1(k)\}$ is proved to clearly modulate in nonictal versus ictal state both in patients with intractable epilepsy and PTZ-treated rodents.

In each state $x \in \{0, 1\}$, the probability function $q_x(\cdot)$ of the observations z_k was history-independent and estimated offline for each session. In particular, for each session, we estimated $q_0(\cdot)$ and $q_1(\cdot)$ by using the sequence z_k from the beginning of the session till the end of the first hand-annotated seizure (30%–50% of the session) via the Baum–Welch's (BW) algorithm [43], [44]. Briefly, given a set $\mathcal{Z}$ of possible values for z_k and a specific (finite) sequence of $R > 0$ observations $(z_1, \ldots, z_R) = (\hat{z}_1, \ldots, \hat{z}_R)$, with $\hat{z}_i \in \mathcal{Z}$ and $i = 1, 2, \ldots, R$, the BW algorithm estimates the probability functions $\hat{q} \triangleq [q_0\ q_1]$ that maximize the expectation of the given sequence $(\hat{z}_1, \ldots, \hat{z}_R)$, i.e., $\hat{q} = \arg\max_q \left[P(z_i = \hat{z}_i,\ i = 1, 2, \ldots, R|q)\right]$.

III. Results

The proposed paradigm achieved similar performances both on simulated and experimental data, and significantly improved over traditional non-optimal detection methods. For each data-set and detection method, two performance measures were considered: (i) the absolute distance $|\overline{T} - T_S|$ between the actual change time $\overline{T}$ and the earliest estimation T_S given by the method, and (ii) the correspondent cumulative loss $J \triangleq G_{T_S}(\pi_{T_S}, 1) + \sum_{i=0}^{T_S-1} G_i(\pi_i, 0)$.

A. Numerical Simulations

We applied our paradigm on both binary (Bernoulli) and continuous (Gaussian) random observations. In both cases, for each train of observations, the *ODP* accurately captured the actual transition time $\overline{T}$ by optimally adapting the detection threshold to the evolution of the *a posteriori* probability π_k [Fig. 2(b) and (g)]. The dynamics of this threshold depends on the length M of the horizon and the relative impact of the expected early and delayed detection in the loss function. For example, if one requires a low number of false positives (i.e., as few early detection cases as possible), the *ODP* threshold will be set to decrease slowly, thus making it more difficult for π_k to cross the threshold and detect a change [see Fig. 2(b) and (g)]. Also, the threshold in (8) depends on the evolution of π_k, i.e.,

it automatically changes based on the current and past values of π_k, thus preventing that eventual isolated peaks in the value of π_k would result in an erroneous change point detection. An example is in Fig. 2(b): the *ODP* threshold (green line) decreases faster during the first 1000 stages (first second, state 0) than the last 1000 stages (seconds 2–3, state 1) because the average value of π_k is smaller in the first case; however, the decrement is not monotonic and sudden increases occur after ~ 700 ms in order to avoid the abrupt peaks of π_k, which are caused by outlier observations of the distribution in state 0.

The dynamical change of the threshold guaranteed that the *ODP* outperformed the classic Bayesian estimation [Fig. 2(b) and (g)], which relies only on the current value of π_k (i.e., no memory involved) and detects a change as soon as the *a posteriori* probability of being in state 1 is higher than the probability of being in state 0 (i.e., $\pi_k > 0.5$).

Also, the *ODP* adaptive threshold works on π_k, which is always in $[0,\ 1]$, instead of the likelihood ratio q_1/q_0 between the probability functions of the observations in state 1 (q_1) and state 0 (q_0), which may significantly vary with the application or the sequence of observations. This is an advantage over the *CUSUM* detector [10], [53], whose state variable g_k explicitly depends on such ratio. Because the *CUSUM* algorithm detects a change point when g_k passes a heuristically chosen and fixed threshold $\overline{g}$ [10], the choice of $\overline{g}$ must depend on the magnitude of g_k in state 0 versus 1 and, therefore, should be manually set for each sequence of observations in order to obtain the best performances [10]. In our case, we used the same $\overline{g}$ for multiple Bernoulli (Gaussian) sequences even though the magnitude of g_k largely varied across them, thus achieving poor detection performances [Fig. 2(b) and (g)], even though, for each set of Bernoulli (Gaussian) sequences, we chose $\overline{g}$ in order to maximize the average *TPR* value across the population of sequences while minimizing the average *FPR* value.

Population-averaged performances for Bernoulli and Gaussian sequences are in Fig. 2(c), (d) and Fig. 2(h), (i), respectively. The *ODP* significantly (t-test, $p < 0.05$) reduced the population-averaged distance $|T_S - \overline{T}|$ between estimated (T_S) and actual change time [Fig. 2(c) and (h)], and provided the minimum value of the loss function [Fig. 2(d) and (i)], thus guaranteeing the optimal balance between the performance goals. Also, distances and losses with *ODP* were significantly lower than with the chance level detector, thus assuring that *ODP* runs better than chance.

B. Movement Onset Detection in PD Patients

Sarma *et al.* [48] reported a significant change in the STN neuronal dynamics at the movement onset. The *ODP* precisely detected such a change in the sequential STN spike train observations in almost every trial [average lag: 1.68 ± 0.5 ms, mean$\pm$ s.e.m., see Fig. 3(c)] independently of the source of the spike trains (i.e., specific STN neuron and PD patient), and guaranteed the smallest value of the loss function (Fig. 3(d). The *ODP* resulted in a very small delay $(< 1$ ms$)$ in case of delayed detection and significantly (t-test, $p < 0.05$) outperformed Bayesian Estimation (*BE*) and *CUSUM* detector. Indeed, in case of delayed detection, the average distance $T_S - \overline{T}$ was 0.79 ± 0.01 ms (*ODP*), 25.8 ± 0.13 ms (*BE*), and 113 ± 1.6 ms (*CUSUM*). In case of early detection, instead, the average distance $\overline{T} - T_S$ was 12.9 ± 0.5 ms (*ODP*), 72 ± 0.67 ms (*BE*), and 69.5 ± 0.69 ms (*CUSUM*). Also, the *ODP* decreased the occurrence of early detections (average: 1 out of 13 trials per neuron (*ODP*) versus 1 out of 2 trials (*BE* and *CUSUM*) and 1 out of 3 trials (*CL*), thus reducing the chance of false positives. In this specific application, frequent early detections would mean poor discrimination capability of movement-specific versus nonmovement-specific changes and would therefore limit the detection specificity.

Performances of the *ODP* were consistent across the whole neuronal population [i.e., low standard error, Fig. 3(c), (d)] and were achieved by capturing the dependency of the probability function q_x on the spiking history H_k in each state $x \in \{0, 1\}$. Such dependency is nonstationary [tools usually used in neuroscience, like the peri-event time histogram, failed in capturing it because they assume that the data is stationary, Fig. 3(e)] characterizes the spiking propensity at each bin [Fig. 3(f)], and differentiates the activity in state 0 versus state 1. However, differences are small [Fig. 3(f)] and this is reflected in the high value of π_k in state 0 and the fluctuations of the *CUSUM* variable g_k around the movement onset [Fig. 3(g)]. In this case, the *ODP* correctly detected the actual onset by modulating up the detection threshold.

C. Early Seizure Detection in PTZ-treated Rodents

Two PTZ-treated rodents developed epileptic seizures. Seven recording sessions and 12 seizures were overall included (two sessions included one seizure each, five sessions had two seizures each, average inter-seizure distance: 208 ± 86.44 s, mean $\pm$ S.D.). iEEG recordings from multiple sites along the thalamo-cortical epileptic pathway were combined and a time-varying power-based connectivity matrix of the sites was computed [Fig. 4(a) and (b)].

For each session, recordings from the beginning till the end of the first clinical seizure were used as training data and the correspondent power-based connectivity matrices were analyzed by computing the first (maximum) singular value σ_1. Results indicate that σ_1 had high modulation at the transition from the non-ictal to the ictal phase [Fig. 4(e)] and a different probability distribution in the two phases [Fig. 4(h)]. Also, because the connectivity matrix combines recordings from cortex (where the seizure is actually recognized), hippocampus and thalamus (where the mechanisms leading to a seizure are presumably activated [49]), the sequence of σ_1 values showed some modulation even before the hand-annotated electrographic onset of the seizures [Fig. 4(a), (b), and (e)].

For each session, we fit the two-state HMM on the (output) sequence of σ_1 values (training data only) and chose state $x = 0$ and $x = 1$ to be the non-ictal and ictal phase, respectively. Then, we estimated the most likely state transition pattern on the remaining data. In this way, we found that the optimal change time from the non-ictal to the ictal distribution of the σ_1 values occurred up to ~ 100 s before the hand-annotated onset $(43.9 \pm 7.6$ s, mean $\pm$ s.e.m.$)$. We used this onset as the reference change point $\overline{T}$ to be detected with the *ODP* [Fig. 4(c), (d), and (f)] and fit the resultant 12 change points with a geometric distribution via maximum likelihood estimation.

With these assumptions, the *ODP* performed better than any other tested approach, even though significant differences at the chosen confidence level $(p < 0.05)$ were achieved only in the comparisons *ODP* versus *CL*, *ODP* versus *CUSUM* [loss value only, Fig. 4(d)], and *ODP* versus heuristic threshold-based (*HT*)

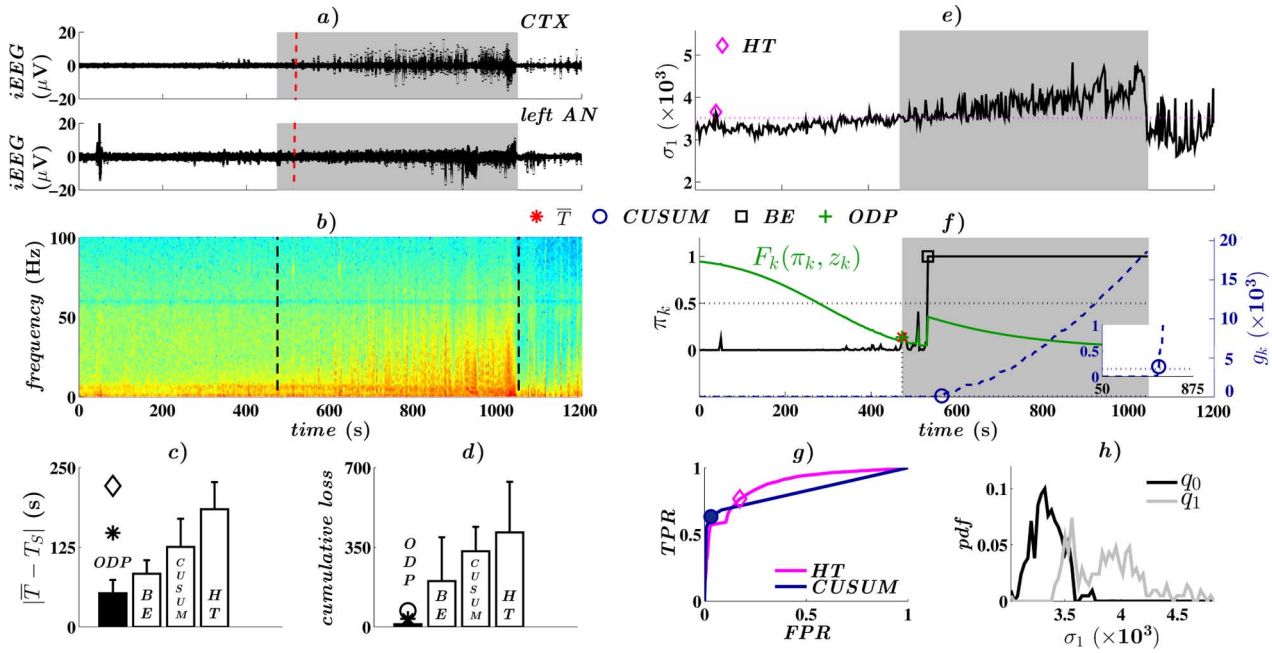

Fig. 4. Early seizure detection in PTZ rodents. (*a*) Intracranial EEG recordings in CTX (top) and left AN (bottom) in one animal. PTZ release starts ~ 60 s after the recording onset (time 0). Background color changes during the ictal state. Electrographic onset (red line) and ictal period are hand-annotated. (*b*) Cross-power spectrum between the iEEG signals in (*a*) with ictal period (dashed lines) correspondent to the gray background in (*a*). (*c*), (*d*) Population-averaged distance and loss as in Fig. 2, respectively. Asterisk, circle, and diamond denote significant difference ($p < 0.05$) *ODP* versus *CL*, *CUSUM*, and *HT* detector, respectively. (*e*) σ_1 (black) for signals in (*a*) and threshold $\overline{h}$ (magenta). The diamond indicates the first window k for which $\sigma_1(k) > \overline{h}$. (*f*) Variable π_k (black), *ODP* threshold $F_k(\cdot)$ (green), *CUSUM* variable g_k (blue dashed), and threshold $\overline{g}$ (blue dotted) for the series in (*e*). Inset: zoom around the estimation given by *CUSUM*. (*g*) Population-averaged ROC curve for *HT* and *CUSUM* detector, respectively. Diamond and circle denote the point of the ROC curve correspondent to $\overline{h}$ and $\overline{g}$ in (*e*) and (*f*), respectively. (*h*) Sample probability function of $z_k = \sigma_1(k)$ in state 0 (non-ictal) and state 1 (ictal). Time scales in (*b*), (*f*) also apply to (*a*), (*e*), respectively.

detector (average distance $|T_S - \overline{T}|$ only, with T_S being the *ODP*-estimated change time, Fig. 4(c)]. Furthermore, the loss function and the absolute distance $|T_S - \overline{T}|$ with *ODP* were smaller than with the other approaches in 12 out of 12 seizures, and the *ODP* threshold was optimally modulated to capture the early changes in the distribution of σ_1, well in advance with respect to the electrographic seizure onsets [Fig. 4(f)].

IV. Discussion

We propose an optimal QD framework for capturing change points in neural observations that are associated with clinical or behavioral state transitions.

Change-point detection is a well-known topic in statistics [1], [10] with recent applications in neuroscience and medicine [15], [17], [62]. However, these applications mainly used spike trains (i.e., binary sequences) and the change points were detected offline, thus combining data from different states and choosing the detection threshold based on the knowledge of the entire neuronal activity. Yu [17] recently applied the QD framework [4], [11], [40], [41] to detect *online* changes in the neuronal spiking rate (which may code different behavioral conditions [62]), but strict assumptions were made (the observations were independent and identically distributed, and the change times $\overline{T}$ followed a geometric distribution). Our approach generalizes the online change point detection problem for neural measurements because it (i) applies both to binary and nonbinary neural sequences, (ii) allows temporal dependencies among consecutive observations (see the examples with the Bernoulli processes and the STN recordings), which is the most likely case in neuroscience applications [48], [59], [62], (iii) does not require a specific type of probability distribution for the change times $\overline{T}$ (which follows from the chosen HMM), and (iv) solves the QD problem via dynamic programming [46], thus resulting in a recursively varying threshold-based detection policy.

The proposed *ODP* is *optimal* in a precise mathematical sense (it minimizes a loss function) [4], [40], performs significantly better than chance, and provides the shortest distance between true and estimated change points and the lowest probability of detecting a change before its actual occurrence. Furthermore, the *ODP* is *adaptive*, i.e., the detection threshold is neither constant (like with the classic Bayesian Estimation) nor chosen *a posteriori* based on the modulation of some statistics in the different states of interest (which is the case in several approaches for seizure detection, e.g., [14], [16], [18], [20], [21], [32], [34]–[36]). The *ODP* threshold is updated at each stage based on the state evolution model, any newly acquired observation, and the modelled temporal dependencies, and this update varies dynamically to prevent that noise-driven abrupt changes of the observation sequence would result in false alarms [Fig. 2(b)].

Finally, the dynamics of the *ODP* threshold is affected by the structure of the loss function J_0 in (2) and the ratio between the weights a_1 and a_2. Thus, differently from the other approaches described above, our framework allows to define the required performances *first* by appropriately constructing the loss function, and *then* design the *ODP* threshold accordingly.

Our framework customizes to the specific application and class of observations by exploiting a time-varying, history-dependent HMM, which can be estimated offline on training data. Also, since the detection policy applies on the Bayesian *a posteriori* probability π_k of state transition, which is always in the range $[0, 1]$, the dynamics of the *ODP* threshold is not explicitly dependent on the average amplitude of the observations in each state. Therefore, the proposed policy can equally work with binary and nonbinary data, and can be applied without further customization to different data generated by the same mechanism across multiple trials. This is a major improvement over classic change-point detection methods in neuroscience (e.g., *CUSUM*, *HT*, etc.). With these methods, indeed, a detection threshold must be set *a priori* and its value must depend on the actual amplitude of the observations (*HT*) or of the log-likelihood ratio (*CUSUM*) in the different states, thus being sensitive to the fluctuations of these variables across multiple trials and triggering more false positives. As an example, we note that, for each PTZ rodent, the singular values of the connectivity matrices largely varied across different recording sessions. As a consequence, in order to fix a threshold for the *HT* and *CUSUM* detector that would work for each session, we backward analysed the sequence of first singular values (*HT*) and the correspondent log-likelihood ratios (*CUSUM*) both before and after each change point (early seizure onset). Then, we set the *CUSUM* and *HT* thresholds to those values that would maximize the true positive rate while minimizing the false positive rate [see Fig. 4(g)]. Despite this optimization (which would not be physically possible anyway, as full knowledge of the sequence of observations would be required), the average distance between actual and detected change time and the number of early detections were large [Fig. 4(c) and (d)], presumably because such optimization did not account for the temporal order of the true and false positives.

We finally note that, because temporal dependencies exist in neural activity, our detection framework automatically adapts to different patterns of sequential observations. For instance, in the movement onset detection example (Fig. 3), the spiking patterns vary across the neuronal population and, for each neuron, across different trials, with no clear separation between rest and movement [Fig. 3(e)]. The neuronal dynamics, however, is captured by the point process model [48] and, for each neuron, the same model parameters fit spike trains collected across several trials. As a consequence, the dynamics of π_k is quite stereotyped across the trials [Fig. 3(g)] and the *ODP* threshold can automatically adapt to the different patterns.

Appendix A
Information State Variable

Given the probability of the initial state, $p_0 \triangleq P(x_0 = 1)$, the conditional probability of state transition, $p_k \triangleq P(x_k = 1|x_{k-1} = 0)$, for all k, and the probability of the output observations $q_x(z|H_k) \triangleq P(z_k = z|x_k = x, H_k)$, for any state $x \in \{0, 1\}$, history $H_k = \{z_0, z_1, \ldots, z_{k-1}\}$, and value z of interest, we have

$$\begin{aligned}\pi_0 &\triangleq P(x_0 = 1|z_0) = \frac{P(x_0 = 1, z_0)}{P(z_0)} \\ &= \frac{q_1(z_0)p_0}{q_1(z_0)p_0 + q_0(z_0)(1 - p_0)}\end{aligned}$$

where we have applied the Bayes' theorem. Similarly, at stage $k = 1$ we have

$$\begin{aligned}\pi_1 &\triangleq P(x_1 = 1|z_0, z_1) = \frac{P(x_1 = 1, z_0, z_1)}{P(z_0, z_1)} \\ &= \frac{P(x_1 = 1, z_0, z_1)}{P(x_1 = 0, z_0, z_1) + P(x_1 = 1, z_0, z_1)} \\ &= \frac{q_1(z_1|z_0)\left[\pi_0 + \xi_0 p_1\right]}{q_0(z_1|z_0)(1 - p_1)\xi_0 + q_1(z_1|z_0)\left[\pi_0 + \xi_0 p_1\right]}\end{aligned} \tag{9}$$

where, denoted with $\overline{T}$ the transition time (change point) and defined $\xi_0 \triangleq 1 - \pi_0$, we have used these facts:

- events $\{x_k = 0\}$ and $\{\overline{T} > k\}$ ($\{x_k = 1\}$ and $\{\overline{T} \leq k\}$) are equivalent for all k;
- $\{\overline{T} > k\} \subseteq \{\overline{T} > k - 1\}$ for all k;
- $P(z_k = z, \overline{T} \geq k + 1) = P(z_k = z, x_k = 0)$ for all k and z, since the current output z_k depends only on the actual state because of the HMM;
- $P(z_k = z, \overline{T} \leq k - 1) = P(z_k = z, x_k = 1)$ for all k and z;
- $P(\overline{T} = k)/P(\overline{T} > k - 1) = P(x_k = 1|x_{k-1} = 0) = p_k$;
- $P(\overline{T} > k)/P(\overline{T} > k - 1) = P(x_k = 0|x_{k-1} = 0) = 1 - p_k$.

Expression (9) is obtained because

$$\begin{aligned}P(x_1 = 0, z_0, z_1) &= P(z_1|z_0, \overline{T} > 1)P(z_0, \overline{T} > 1) \\ &= q_0(z_1|z_0)P(z_0|x_0 = 0)P(\overline{T} > 1) \\ &= q_0(z_1|z_0)\frac{P(x_0 = 0|z_0)P(z_0)}{P(\overline{T} > 0)}P(\overline{T} > 1) \\ &= q_0(z_1|z_0)(1 - p_1)\xi_0 P(z_0) \\ P(x_1 = 1, z_0, z_1) &= P(z_1|z_0, x_1 = 1)P(z_0, \overline{T} \leq 1) \\ &= q_1(z_1|z_0)\left[P(\overline{T} \leq 0, z_0)\right. \\ &\qquad \left. + P(\overline{T} = 1, z_0)\right] \\ &= q_1(z_1|z_0)\left[P(x_0 = 1|z_0)P(z_0)\right. \\ &\qquad \left. + P(z_0|\overline{T} = 1)P(\overline{T} = 1)\right] \\ &= q_1(z_1|z_0)\left[\pi_0 P(z_0)\right. \\ &\qquad \left. + P(z_0|x_0 = 0)P(\overline{T} = 1)\right] \\ &= q_1(z_1|z_0)\left[\pi_0 P(z_0)\right. \\ &\qquad \left. + \frac{P(x_0 = 0|z_0)P(z_0)}{P(\overline{T} > 0)}P(\overline{T} = 1)\right] \\ &= q_1(z_1|z_0)\left[\pi_0 + \xi_0 p_1\right]P(z_0).\end{aligned}$$

By introducing $L_1 \triangleq q_1(z_1|z_0)/q_0(z_1|z_0)$ we can finally write

$$\pi_1 = \frac{L_1\left[\pi_0 + \xi_0 p_1\right]}{(1 - p_1)\xi_0 + L_1\left[\pi_0 + \xi_0 p_1\right]}.$$

Similarly, it is straightforward to show that for $L_k \triangleq q_1(z_k|H_k)/q_0(z_k|H_k)$ we have

$$\begin{aligned}\pi_{k+1} &= \frac{L_{k+1}\left[\pi_k + \xi_k p_{k+1}\right]}{(1 - p_{k+1})\xi_k + L_{k+1}\left[\pi_k + \xi_k p_{k+1}\right]} \\ &\triangleq \Phi_{k+1}(\pi_k, z_{k+1}, H_{k+1}).\end{aligned} \tag{10}$$

APPENDIX B
POINT PROCESS MODELS OF STN NEURONS

Each STN neuron in our dataset was modelled as a point process both before and during movement, and the conditional probability of a spike in a given bin k depends on the spiking activity H_k in the last 150 bins before k. For each neuron and state $x \in \{0, 1\}$, the relationship between the instantaneous rate (i.e., the conditional intensity function λ_x) and the spiking history was captured by a generalized linear model [60]

$$\log \lambda_x(k|H_k) = \alpha_x + \sum_{i=1}^{10} \beta_{x,i} N(k-i+1:k-i) + \sum_{j=1}^{14} \gamma_{x,j} N\big(k-10(j+1):k-10j\big) \quad (11)$$

where $N(a:b) \triangleq \sum_{r=a}^{b} z_r$ is the number of spikes in the bins from a to b, and $\Theta_x = \left[\alpha_x, \{\beta_{x,i}\}_{i=1}^{10}, \{\gamma_{x,j}\}_{j=1}^{14}\right]$ is estimated separately for $x \in \{0, 1\}$ on training data (50% of the trials for each neuron in Table I) via maximum likelihood [59]. Motivations and further explanation of these models are in [48].

ACKNOWLEDGMENT

Experiments with PD patients were conducted in collaboration with M. L. Cheng, Z. M. Williams, and R. Hu at Massachusetts General Hospital. Experiments with PTZ-treated rats were conducted in collaboration with M. A. Mirski at Johns Hopkins School of Medicine.

REFERENCES

[1] G. B. Wetherhil and D. W. Brown, *Statistical Process Control*. London, U.K.: Chapman Hall, 1991.
[2] R. Trivedi and R. Chandramouli, "Secret key estimation in sequential steganography," *IEEE Trans. Signal Process.*, vol. 53, no. 2, pp. 746–757, 2005.
[3] A. G. Tartakovsky, B. L. Rozovskii, R. B. Blazek, and H. Kim, "A novel approach to detection of intrusions in computer networks via adaptive sequential and batch-sequential change-point detection methods," *IEEE Trans. Signal Process.*, vol. 54, no. 9, pp. 3372–3382, Sep. 2006.
[4] A. N. Shiryaev, H. Geman, D. Madan, S. Pliska, and T. Vorst, Eds., "Quickest detection problems in the technical analysis of financial data," in *Mathematical Finance—Bachelier Congress 2000*, Berlin, Germany, 2002, pp. 487–521.
[5] E. Andreou and E. Ghysels, "The impact of sampling frequency and volatility estimators on change point tests," *J. Financial Econ.*, vol. 2, pp. 290–318, 2004.
[6] M. Pettersson, "Monitoring a freshwater fish population: Statistical surveillance of biodiversity," *Environmetrics*, vol. 9, pp. 139–150, 1998.
[7] T. P. Barnett, D. W. Pierce, and R. Schnur, "Detection of anthropogenic climate change in the world's oceans," *Science*, vol. 292, pp. 270–274, 2001.
[8] G. J. Gibson, A. Kleczkowski, and C. A. Gilligan, "Bayesian analysis of botanical epidemics using stochastic compartmental models," *Proc. Natl. Acad. Sci. USA*, vol. 101, pp. 12120–12124, 2004.
[9] B. K. Ellis *et al.*, "Long-term effects of a trophic cascade in a large lake ecosystem," *Proc Natl. Acad. Sci. USA*, vol. 108, pp. 1070–1075, 2011.
[10] M. Basseville and I. V. Nikiforov, *Detection of Abrupt Changes: Theory and Applications*. Englewood Cliffs, NJ: Prentice Hall, 1993.
[11] H. V. Poor and O. Hadjiliadis, *Quickest Detection*. Cambridge, U.K.: Cambridge Univ. Press, 2009.
[12] N. V. Thakor, Y. S. Zhu, and K. Y. Pan, "Ventricular tachycardia and fibrillation detection by a sequential hypothesis testing algorithm," *IEEE Trans. Biomed. Eng.*, vol. 37, no. 9, pp. 837–843, Sep. 1990.
[13] N. V. Thakor, A. Natarajan, and G. F. Tomaselli, "Multiway sequential hypothesis testing for tachyarrhythmia discrimination," *IEEE Trans. Biomed. Eng.*, vol. 41, no. 5, pp. 480–487, May 1994.
[14] I. Osorio, M. G. Frei, and S. B. Wilkinson, "Real-time automated detection and quantitative analysis of seizures and short-term prediction of clinical onset," *Epilepsia*, vol. 39, pp. 615–627, 1998.
[15] J. Ushiba, Y. Tomita, Y. Masakado, and Y. Komune, "A cumulative sum test for a peri-stimulus time histogram using the Monte Carlo method," *J. Neurosci. Methods*, vol. 118, pp. 207–214, 2002.
[16] A. M. White *et al.*, "Efficient unsupervised algorithms for the detection of seizures in continuous EEG recordings from rats after brain injury," *J. Neurosci. Methods*, vol. 152, pp. 255–266, 2006.
[17] A. J. Yu, "Optimal change-detection and spiking neurons," in *Proc. 20th Annu. Conf. Neural Inf. Process. Syst. (NIPS 2006)*, Vancouver, BC, Canada, 2006, pp. 1545–1552.
[18] A. Shoeb *et al.*, "Patient-specific seizure onset detection," *Epilepsy Behav.*, vol. 5, pp. 483–498, 2004.
[19] J. Hu, J. Si, B. P. Olson, and J. He, "Feature detection in motor cortical spikes by principal component analysis," *IEEE Trans. Neural Syst. Rehab Eng.*, vol. 13, no. 3, pp. 256–262, Sep. 2005.
[20] M. J. van Putten, T. Kind, E. Visser, and V. Lagerburg, "Detecting temporal lobe seizures from scalp EEG recordings: A comparison of various features," *Clin. Neurophysiol.*, vol. 116, pp. 2480–2489, 2005.
[21] R. Meier, H. Dittrich, A. Schulze-Bonhage, and A. Aertsen, "Detecting epileptic seizures in long-term human EEG: A new approach to automatic online and real-time detection and classification of polymorphic seizure patterns," *J. Clin. Neurophysiol.*, vol. 25, pp. 119–131, 2008.
[22] M. Tito, M. Cabrerizo, M. Ayala, P. Jayakar, and M. Adjouadi, "Seizure detection: An assessment of time- and frequency-based features in a unified two-dimensional decisional space using nonlinear decision functions," *J. Clin. Neurophysiol.*, vol. 26, pp. 381–391, 2009.
[23] J. W. Yoon, S. J. Roberts, M. Dyson, and J. Q. Gan, "Adaptive classification for brain computer interface systems using sequential Monte Carlo sampling," *Neural Netw.*, vol. 22, pp. 1286–1294, 2009.
[24] J. J. Baker, E. Scheme, K. Englehart, D. T. Hutchinson, and B. Greger, "Continuous detection and decoding of dexterous finger flexions with implantable myoelectric sensors," *IEEE Trans. Neural Syst. Rehab. Eng.*, vol. 18, no. 4, pp. 424–432, Aug. 2010.
[25] A. Temko, E. Thomas, W. Marnane, G. Lightbody, and G. Boylan, "EEG-based neonatal seizure detection with support vector machines," *Clin. Neurophysiol.*, vol. 122, pp. 464–473, 2011.
[26] A. Alkan, E. Koklukaya, and A. Subasi, "Automatic seizure detection in EEG using logistic regression and artificial neural network," *J. Neurosci. Methods*, vol. 148, pp. 167–176, 2005.
[27] S. B. Wilson, "A neural network method for automatic and incremental learning applied to patient-dependent seizure detection," *Clin. Neurophysiol.*, vol. 116, pp. 1785–1795, 2005.
[28] S. Ghosh-Dastidar, H. Adeli, and N. Dadmehr, "Mixed-band wavelet-chaos-neural network methodology for epilepsy and epileptic seizure detection," *IEEE Trans. Biomed. Eng.*, vol. 54, no. 9, pp. 1545–1551, Sep. 2007.
[29] V. Srinivasan, C. Eswaran, and N. Sriraam, "Approximate entropy-based epileptic EEG detection using artificial neural networks," *IEEE Trans. Inf. Technol. Biomed.*, vol. 11, no. 3, pp. 288–295, May 2007.
[30] S. Acharya *et al.*, "Decoding individuated finger movements using volume-constrained neuronal ensembles in the M1 hand area," *IEEE Trans. Neural Syst. Rehab. Eng.*, vol. 16, no. 1, pp. 15–23, Feb. 2008.
[31] S. Ghosh-Dastidar, H. Adeli, and N. Dadmehr, "Principal component analysis-enhanced cosine radial basis function neural network for robust epilepsy and seizure detection," *IEEE Trans. Biomed. Eng.*, vol. 55, no. 2, pp. 512–518, Feb. 2008.
[32] L. Guo, D. Rivero, J. Dorado, J. R. Rabunal, and A. Pazos, "Automatic epileptic seizure detection in EEGs based on line length feature and artificial neural networks," *J. Neurosci. Methods*, vol. 191, pp. 101–109, 2010.
[33] D. Sussillo *et al.*, "A recurrent neural network for closed-loop intracortical brain-machine interface decoders," *J. Neural Eng.*, vol. 9, p. 026027, 2012.
[34] Y. U. Khan and J. Gotman, "Wavelet based automatic seizure detection in intracerebral electroencephalogram," *Clin. Neurophysiol.*, vol. 114, pp. 898–908, 2003.

[35] S. Grewal and J. Gotman, "An automatic warning system for epileptic seizures recorded on intracerebral EEGs," *Clin. Neurophysiol.*, vol. 116, pp. 2460–2472, 2005.
[36] M. E. Saab and J. Gotman, "A system to detect the onset of epileptic seizures in scalp EEG," *Clin. Neurophysiol.*, vol. 116, pp. 427–442, 2005.
[37] C. Kemere *et al.*, "Detecting neural-state transitions using hidden Markov models for motor cortical prostheses," *J. Neurophysiol.*, vol. 100, pp. 2441–2452, 2008.
[38] G. Schalk, P. Brunner, L. A. Gerhardt, H. Bischof, and J. R. Wolpaw, "Brain computer interfaces (BCIs): Detection instead of classification," *J. Neurosci. Methods*, vol. 167, pp. 51–62, 2008.
[39] P. Miller and D. B. Katz, "Stochastic transitions between neural states in taste processing and decision-making," *J. Neurosci.*, vol. 30, pp. 2559–2570, 2010.
[40] A. N. Shiryaev, "On optimum methods in quickest detection problems," *Theory Probab. Appl.*, vol. 8, pp. 22–46, 1963.
[41] H. V. Poor, "Quickest detection with exponential penalty for delay," *Ann. Statist.*, vol. 26, pp. 2179–2205, 1998.
[42] H. C. Lee, W. van Drongelen, A. B. McGee, D. M. Frim, and M. H. Kohrman, "Comparison of seizure detection algorithms in continuously monitored pediatric patients," *J. Clin. Neurophysiol.*, vol. 24, pp. 137–146, 2007.
[43] R. J. Elliott, L. Aggoun, and J. B. Moore, *Hidden Markov Models. Estimation and Control*. New York: Springer, 1995.
[44] R. Durbin, S. Eddy, A. Krogh, and G. Mitchison, *Biological Sequence Analysis*. Cambridge, U.K.: Cambridge University Press, 1998.
[45] J. O. Berger, *Statistical Decision Theory and Bayesian Analysis*, 2nd ed. New York: Springer, 1985.
[46] D. P. Bertsekas, *Dynamic Programming and Optimal Control*, 3rd ed. Belmont, MA: Athena Scientific, 2005.
[47] P. R. Freeman, "The secretary problem and its extensions: A review," *Int. Stat. Rev.*, vol. 51, pp. 189–206, 1983.
[48] S. V. Sarma *et al.*, "Using point process models to compare neural spiking activity in the subthalamic nucleus of Parkinson's patients and a healthy primate," *IEEE Trans. Biomed. Eng.*, vol. 57, no. 6, pp. 1297–1305, Jun. 2010.
[49] D. L. Sherman *et al.*, "Sinusoidal modeling of ictal activity along a thalamus-to-cortex seizure pathway. I: New coherence approaches," *Ann. Biomed. Eng.*, vol. 32, pp. 1252–1264, 2004.
[50] H. Bergman, T. Wichmann, B. Karmon, and M. R. DeLong, "The primate subthalamic nucleus. II. Neuronal activity in the MPTP model of Parkinsonism," *J. Neurophysiol.*, vol. 72, pp. 507–520, 1994.
[51] Z. M. Williams, J. S. Neimat, G. R. Cosgrove, and E. N. Eskandar, "Timing and direction selectivity of subthalamic and pallidal neurons in patients with Parkinson's disease," *Exp. Brain Res.*, vol. 162, pp. 407–416, 2005.
[52] J. T. Gale, D. C. Shields, F. A. Jain, R. Amirnovin, and E. N. Eskandar, "Subthalamic nucleus discharge patterns during movement in the normal monkey and Parkinsonian patient," *Brain Res.*, vol. 1260, pp. 15–23, 2009.
[53] E. S. Page, "Continuous inspection schemes," *Biometrika*, vol. 41, pp. 100–115, 1954.
[54] S. Santaniello, D. L. Sherman, M. A. Mirski, N. V. Thakor, and S. V. Sarma, "A Bayesian framework for analyzing iEEG data from a rat model of epilepsy," in *Proc. 33rd IEEE EMBS Annu. Conf. (EMBC 2011)*, Boston, MA, 2011, pp. 1435–1438.
[55] S. V. Sarma and S. Santaniello, "Quickest detection of state-transition in point processes: Application to neuronal activity," in *Proc. 18th IFAC World Conference (IFAC 2011)*, Milan, Italy, 2011, pp. 10021–10026.
[56] S. Santaniello *et al.*, "Quickest detection of drug resistant seizures: An optimal control approach," *Epilepsy Behav.*, vol. 22, pp. S49–S60, 2011.
[57] T. Fawcett, "An introduction to ROC analysis," *Pattern Recognit. Lett.*, vol. 27, pp. 861–874, 2006.
[58] D. L. Snyder and M. I. Miller, *Random Point Processes in Time and Space*. New York: Springer, 1991.
[59] E. N. Brown, R. Barbieri, U. T. Eden, and L. M. Frank, "Likelihood methods for neural data analysis," in *Computational Neuroscience: A Comprehensive Approach*, J. Feng, Ed. London, U.K.: CRC, 2003, pp. 253–286.
[60] P. McCullagh and J. A. Nelder, *Generalized Linear Models*, 2nd ed. Boca Raton, FL: CRC, 1990.
[61] H. G. Golub and C. F. van Loan, *Matrix Computations*, 3rd ed. Baltimore, MD: Johns Hopkins Univ. Press, 1996.
[62] J. W. Pillow, Y. Ahmadian, and L. Paninski, "Model-based decoding, information estimation, and change-point detection techniques for multineuron spike trains," *Neural Comput.*, vol. 23, pp. 1–45, 2011.

Sabato Santaniello (S'02–M'08) received the Laurea degree in computer engineering with honours from Università di Napoli Federico II, Napoli, Italy, in 2004, and the Ph.D. degree in information engineering from Università del Sannio, Benevento, Italy, in 2007.

He is Postdoctoral Fellow at the Department of Biomedical Engineering, Johns Hopkins University, Baltimore, MD. His research interests include computational neuroscience, modelling and estimation of neural systems, and neural control, with applications to deep brain stimulation, responsive neural stimulation, and seizure onset detection.

David L. Sherman (S'83–M'93) received the A.B. degree in psychology from Columbia University, New York, in 1980, the B.S.E.E. degree from Florida Atlantic University, Boca Raton, in 1983, and the M.S. and Ph.D. degrees in electrical engineering from Purdue University, West Lafayette, IN.

He is currently the Chief Scientific Officer at Infinite Biomedical Technologies, a company he co-founded with postdoctoral mentor, Dr. Nitish Thakor and his graduate student, Dr. Ananth Natarajan. He was a Research Assistant Professor in the Department of Biomedical Engineering, Johns Hopkins University, Baltimore, MD. His research interests include biological signal analysis and statistical signal processing.

Dr. Sherman received a Whitaker postdoctoral fellowship in 1993 and a Mc Donnell-Pew Fellowship in cognitive neuroscience in 1995 for research at Johns Hopkins University. He is the recipient of the "Engineer of the Year" Award in 2005 from the Engineering Society of Baltimore.

Nitish V. Thakor (F'94) received the B.Tech. degree in electrical engineering at the Indian Institute of Technology, Bombay, India, in 1974, and the M.S. degree in biomedical engineering and the Ph.D. degree in electrical and computer engineering at the University of Wisconsin, Madison, in 1978 and 1981, respectively.

He is a Professor of Biomedical Engineering, Electrical and Computer Engineering, and Neurology at Johns Hopkins University, Baltimore, MD, and directs the Laboratory for Neuroengineering in the same university. His technical expertise is in the areas of neural diagnostic instrumentation, neural microsystems, neural signal processing, optical imaging of the nervous system, rehabilitation, neural control of prosthesis, and brain machine interface. He is the Director of a Neuroengineering Training program funded by the National Institute of Health. He has published 225 refereed journal papers, generated 11 patents, co-founded four companies, and carries out research funded mainly by the National Institutes of Health (NIH), National Science Foundation (NSF), and Defense Advanced Research Projects Agency.

Dr. Thakor was the Editor-in-Chief of IEEE TRANSACTIONS ON NEURAL SYSTEMS AND REHABILITATION ENGINEERING (2005–2011). He is the recipient of a Research Career Development Award from the NIH and a Presidential Young Investigator Award from the NSF, and is a Fellow of the American Institute of Medical and Biological Engineering and Founding Fellow of the Biomedical Engineering Society, Technical Achievement Award from IEEE and Distinguished Alumnus award from Indian Institute of Technology, Bombay and University of Wisconsin, Madison.

Emad N. Eskandar received the B.A. degree in chemistry from the University of Nebraska, Lincoln, in 1987, and the M.D. degree from the University of Southern California, Los Angeles, in 1993.

From 1989 to 1991, he was a Fellow in Neurophysiology, National Institutes of Health, Bethesda, MD. From 1993 to 1999, he was a Resident in Neurosurgery, Massachusetts General Hospital, Boston. From 1996 to 1998, he was a Postdoctoral Fellow in Neurophysiology, Harvard Medical School, Cambridge, MA. He is currently a Neurosurgeon at the Massachusetts General Hospital and an Associate Professor of Surgery at Harvard Medical School. He is involved in multidisciplinary programs and also in psychiatry, neurology, and anaesthesia. He is also engaged in cutting-edge surgical treatments for movement disorders, epilepsy, pain, and severe psychiatric disorders. He is involved in basic research laboratory, where he is engaged in theories of learning, motivation, depression, and drug addiction.

Sridevi V. Sarma (M'04) received the B.S. degree in electrical engineering from Cornell University, Ithaca, NY, in 1994, and the M.S. and Ph.D. degrees in electrical engineering and computer science from the Massachusetts Institute of Technology, Cambridge, in 1997 and 2006, respectively.

She was a Postdoctoral Fellow in the Brain and Cognitive Sciences Department, Massachusetts Institute of Technology, Cambridge, from 2006 to 2009. She is now an Assistant Professor in the Institute for Computational Medicine, Department of Biomedical Engineering, Johns Hopkins University, Baltimore, MD. Her research interests include modelling, estimation, and control of neural systems.

Dr. Sarma is a recipient of the GE faculty for the future scholarship, the National Science Foundation graduate research fellow, the L'Oreal For Women In Science fellow, the Burroughs Wellcome Fund Careers at the Scientific Interface Award, the NSF CAREER award, and the Presidential Early Career Award for Scientists and Engineers (PECASE).